Article

Cryo-nanoimaging of single human macrophage cells: 3D structural and chemical quantification

Chiara Gramaccioni, Yang Yang, Alexandra Pacureanu, Nicola Viganò, Alessandra Procopio, Piera Valenti, Luigi Rosa, Francesca Berlutti, Sylvain Bohic, and Peter Cloetens

Anal. Chem., **Just Accepted Manuscript** • DOI: 10.1021/acs.analchem.9b04096 • Publication Date (Web): 12 Mar 2020

Cryo-nanoimaging of single human macrophage cells: 3D structural and chemical quantification

Chiara Gramaccioni,*,† Yang Yang,‡ Alexandra Pacureanu,‡ Nicola Vigano,‡ Alessandra Procopio,¶ Piera Valenti,§ Luigi Rosa,§ Francesca Berlutti,§ Sylvain Bohic,*,‡,‖ and Peter Cloetens*,‡

†*University of Calabria, Department of Physics, 87036 Arcavata di Rende, Italy*
‡*ESRF, The European Synchrotron, 38043 Grenoble, France*
¶*University of Bologna, Department of Pharmacy and biotechnology,40127 Bologna Italy*
§*University of Sapienza Roma, Department of Public Health and Infectious Diseases, 00185 Roma Italy*
‖*Universite Grenoble Alpes, EA-7442 Rayonnement Synchrotron et Recherche Medicale, 38043 Grenoble, France*

E-mail: chiara.gramaccioni@gmail.com; bohic@esrf.eu; cloetens@esrf.eu

Abstract

X-ray microscopy is increasingly used in biology, but in most cases only in a qualitative way. We present here a 3D correlative cryo X-ray microscopy approach suited for the quantification of molar concentrations and structure in native samples at nanometer scale. The multi-modal approach combines X-ray fluorescence and X-ray holographic nanotomography on 'thick' frozen-hydrated cells. The quantitativeness of the X-ray fluorescence reconstruction is improved by estimating the self-attenuation from the 3D holography reconstruction. Applied to complex macrophage cells, we extract the quantification of major and minor elements heavier than phosphorous, as well as the density, in the different organelles. The intracellular landscape shows remarkable elemental differences. This novel analytical microscopy approach will be of particular interest to investigate complex biological and chemical systems in their native environment.

Many elements are essential for life. In particular, metal ions play a vital role in many key biological and biochemical cellular reactions as nearly one third of proteins need to bind metals for their function and/or to stabilize their structure.[1] Investigating metal homeostasis and its dysfunctions is crucial to better understand the cell functions and the influence on cellular pathology.[2,3] The associated challenge to analytical chemistry techniques, consists in locating and quantifying these elements, mostly present at trace level, within the highly complex intracellular landscape. The advent decades ago of transmission electron microscopy (TEM) and cryo-electron microscopy (cryo-EM) allows to explore the complex intracellular structure of cells.[4] Coupled to X-ray micro-analysis, it allows to probe the elemental content on portions of ultrathin cellular sections. The unsurpassed resolution of TEM allows to resolve organelles and the finest structures such as membranes or intermediate filaments. Elemental analysis of cells can now be performed in two dimensions by several elemental mapping methods, which mainly differ in sensitivity and spatial resolution attainable,[5] but 3D information is lacking. Complementary, 3D energy-filtered transmission electron microscopy (EFTEM) allows tomographic chemical maps at nanome-

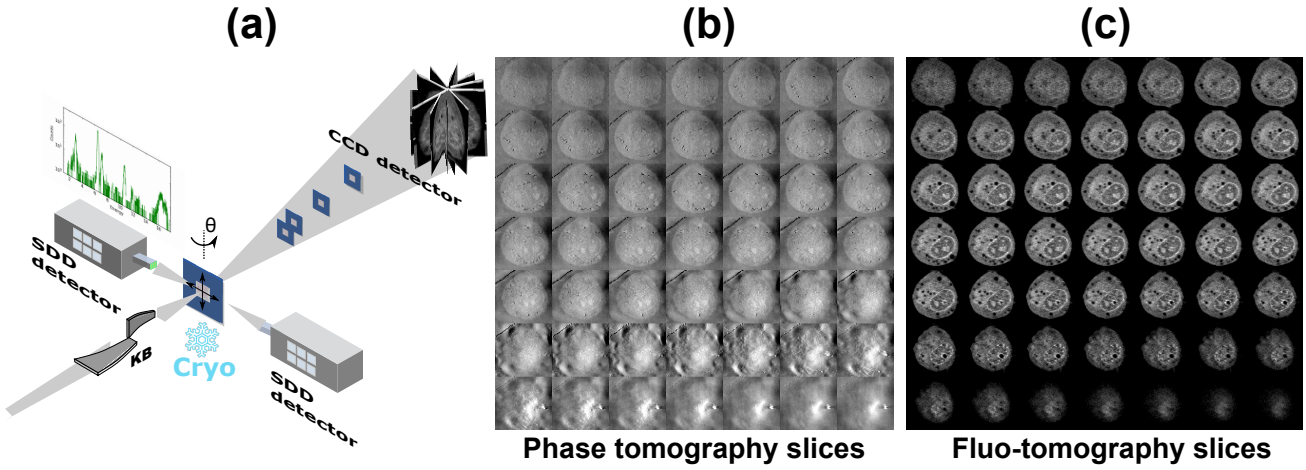

Figure 1: (a) Schematic of the experimental setup for cryo correlative X-ray holographic and X-ray fluorescence nanotomography. An animated video showing the X-ray fluorescence projections of eight main elements is attached in Video 1. (b) A selected range of the reconstructed X-ray phase tomography slices. (c) Reconstructed X-ray fluorescence tomography slices of one element (phosphorous) in the corresponding range.

ter scale of some intracellular compartment on 50-100 nm ultrathin cellular sections.[6,7] This technique, as well as nanoscale secondary ion mass spectrometry (nanoSIMS), requires however tedious sample preparation and manipulation.[8] Despite many efforts, no electron microscopy technique was able to provide 3D elemental analysis of entire cells. 3D time-of-flight secondary ion mass spectrometry (TOF-SIMS) has been demonstrated to provide 3D molecular imaging at the single cell level, but at limited lateral resolution and in a destructive way.[9]

X-ray tomography techniques offer the potential to image and quantify 'thick' cells and tissues in 3D without excessive sample preparation. In particular, X-ray fluorescence (XRF) tomography has been used to quantify the 3D elemental content in air-dried diatoms.[10] Correlative microscopy approaches can obtain the complementary structural information through the use of a phase contrast technique. For this goal X-ray ptychography has been used in the qualitative evaluation of elemental content in frozen-hydrated green algae.[11] Our group recently reported the use of correlative synchrotron X-ray holographic and X-ray fluorescence nanotomography to quantify the elemental 3D distribution within fixed or freeze-dried single cells at room-temperature.[12,13] The major component of cells is water that is not compatible with high resolution elemental analysis due to radiation damage. The gold standard method uses cryo-preservation in order to analyse cells in their near-native state, i.e. frozen hydrated (within vitrified water). In this study, we use correlative synchrotron X-ray holographic and X-ray fluorescence nanotomography to obtain the 3D molar concentration and density in single frozen-hydrated human macrophage cells. The complex macrophage cell is characteristic for many biological cases with trace element concentrations and small density structural changes. Opposed to a previous study conducted at a low X-ray energy of 5.5 keV,[11] the high X-ray energy used here (17 keV) is crucial to detect essential trace metals such as Fe-Zn with excellent sensitivity in XRF, while X-ray holography preserves the structural information on weakly scattering samples. Indeed, the role of metal ions such as zinc, copper and iron in macrophages is still a matter of debate.[14–16] In this context, we quantify and correlate the fundamental elements and the mass density in distinct macrophage organelles.

Human macrophage cells were cultured in RPMI 1640 medium (Euroclone, Italy) supplemented with 10 % calf serum, and grown on 500 nm thick Si_3N_4 membranes supported by

5 x 5 mm^2 silicon frames. The cells were stimulated by lipopolysaccharide (LPS)[17] that triggers macrophage activation of inflammatory cytokine expression. To safeguard the cellular structure and elemental content, the cells were cryofixed by plunge freezing in liquid ethane.[18] The acquisition protocol of correlative cryo X-ray tomography at the ID16A nano-imaging beamline[19] of the ESRF is schematically depicted in Figure 1a. First X-ray holographic nanotomography was performed consisting of the acquisition using an indirect CCD based detector of four full-field tomography scans with the sample at different distances downstream of the nanofocus.[20] Phase retrieval allowed to convert the in-line holograms at different defocus to quantitative phase maps with a pixel size of 40 nm and a field of view of 80 μm. A large number of these projections at different angles (1800) were used to reconstruct the real part of the refractive index decrement using an analytic tomography reconstruction algorithm.[21] Under the Guinier approximation valid for low Z materials,[22,23] the refractive index decrement was converted into local mass density. Figure 1b shows a number of the obtained virtual slices through the density distribution of the cell. X-ray fluorescence tomography was performed next and consists in acquiring 2D X-ray fluorescence maps at a limited number of angles (30). Each map is acquired on-the-fly while scanning the sample through the nanofocus and collecting full X-ray fluorescence emission spectra with one six-element silicon drift diode detector. The maps were converted through a calibrated fit to areal mass density maps for fifteen elements. Due to the longer acquisition time, a coarser pixel size was used for XRF (120 and 130 nm pixel size for the cell shown in Figure 2 and Figure S2, respectively). 3D elemental concentration maps were reconstructed using the iterative tomographic reconstruction algorithm Chambolle-Pock with Kullback-Liebler data-fidelity,[24] and the attenuation correction approach described in Vigano et al.[25] In order to determine the attenuation of the X-ray fluorescence emission we have segmented the quantitative 3D data obtained from the phase imaging modality. This quantification is based on known approximate compositions of the cell/ice and of the silicon nitride membrane. Alternative multimodal reconstruction schemes have been proposed.[26–28] Figure 1c shows as an example the obtained virtual slices through the phosphorous distribution of the cell. Further details of the acquisition and reconstruction are reported in the Supporting Information.

Results of the correlative tomography approach are shown in Figure 2 on the central slice through the macrophage cell. An animated video showing volume renderings corresponding to Figure 2b and c is attached in Video 4. Compared to the individual 2D projections (see Figure S1) a striking gain in spatial resolution can be noted thanks to the depth information provided by the tomographic reconstruction. Furthermore, elements with low concentrations such as Mn (0.8 mM maximum) and Ca (4 mM maximum) are clearly localized in space, while they are hardly detectable in the individual projections. As a result, the molar concentration distributions of major and minor elements can be compared and colocalizations can be investigated. Furthermore, these elemental distributions can be correlated with the mass density distribution through the entire cell. Very heterogeneous distributions are found for several elements associated with the different organelles. We performed a manual 3D segmentation with the Fiji[29] Segmentation_Editor plugin dividing the cell in different compartments: vacuoles and nucleoli using the density map, cytoplasm, 'endoplasmic reticulum including Golgi' (ERGolgi), nucleus, nuclear membrane using the P map, 'Golgi' using the Zn map. The identification of the ER and Golgi compartments is hypothetical as the spatial resolution does not allow to resolve the fine organelle structures. A comparison of the central slice of respectively the density, the Zn concentration, the P concentration and the segmented cell compartments is reported in Figure S3, as well as the animation Video 5 showing all slices. Based on this segmentation, the average and standard deviation of the molar concentrations and density in the different compartments are presented in Figure 3. Extended numerical values of the organelle quantification are re-

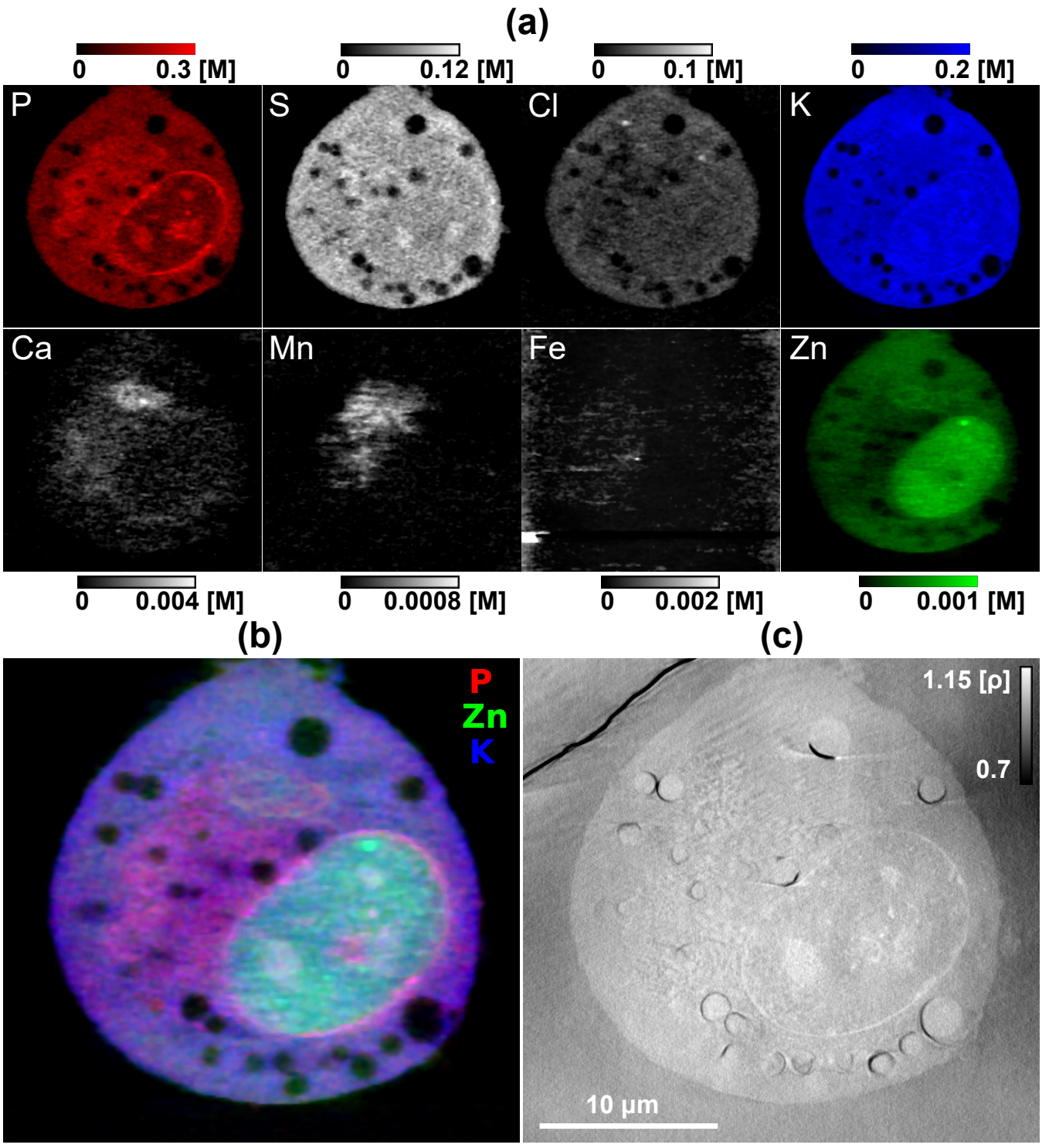

Figure 2: Correlative cryo X-ray tomography applied to a macrophage cell. (a) Central tomography slice of the molar concentration for eight main elements. An animation video with all molar concentration slices is attached in Video 2. (b) Composite tomography slice combining the P, Zn and K concentrations. (c) Corresponding tomography slice of the mass density distribution. An animation video with all density slices is attached in Video 3.

ported in Tables S3-S11. A volume rendering using the UCSF Chimera software[30] of the segmented organelles is shown in Figure 3b. The reconstruction of the intracellular Fe distribution is strongly perturbed by the presence of extracellular Fe from the cell culture. The associated hotspots and the general Fe background of the experimental environment hampers the detection of diffuse Fe signals in specific organelles. For this reason the Fe quantification is not shown in Figure 3. The P molar concentration shows highest levels in the nucleoli and around the nucleus with an increase of 70-85 % compared to the cytoplasm, while the ER-Golgi and Golgi compartments show an increase of about 40 %. The phosphorus distribution is indicative of mainly nucleic acids, phosphorylated proteins and phospholipids of the nucleus.[31] The observed distribution of phosphorus is similar to that reported on ultrathin cellular sections using nano-scale secondary ion mass spectrometry: while P-rich and S-rich common regions indicate nucleoli regions, P-rich but not S-rich regions in the nucleus are indicative of the chromatin regions.[32] The P-ring around the nucleus is interpreted as the chromatin rim that is connected to the nuclear envelope.[33] The S distribution is rather homogeneous inside the cell with increased levels in the nucleoli (24 %) and Golgi compartment (19 %) compared to the cytoplasm. Similarly, the Cl distribution is homogeneous except for increased levels in the Golgi compartment (21 %). As visible in Video 2, small Cl-rich vesicles, with a diameter of about 250 nm, stand out in the cytoplasm. They show Cl concentrations up to 0.11 M compared to the cytoplasm average of 0.019 M. It has been shown that Cl plays a role in cell growth and differentiation but also in the regulation of pH and in cell processes regulating cell volume.[34] Indeed, chloride channels have been found in various major organelles such as the endoplasmic reticulum and the Golgi, mitochondria, endosomes and lysosomes, nucleus, and cell vesicles.[35] Chlorine being involved in the acidification of organelles and the small size of the observed Cl-rich vesicles suggest that it could correspond to lysosomes having a typical diameter of 200 - 300 nm.[36] While homogeneous at coarser resolutions, the K distribution shows some heterogeneity in the nucleoli (35 % increase) and the nuclear membrane (29 % increase). The trace elements Ca and Mn are particularly absent from the cytoplasm and are mainly located in the ER and the Golgi compartments. While Mn has identical levels in ER and Golgi, Ca shows more than two times higher concentrations (1.6 mM) in the compartment identified as Golgi compared to the ER with Golgi. The Golgi apparatus is known to participate in the regulation of cytosolic Ca^{2+} and being an important intracellular Ca^{2+} store with relatively high concentration in the 1-2 mM range.[37] This agrees well with the total Ca concentration we report here, as well as in ER where values in the 10^{-4} range are reported.[38] Mn is known to be present in the Golgi and of particular importance for the correct glycosylation of the secretory proteins.[39] Zn is present in relatively low concentrations with a cell average of 0.28 mM, but it clearly stands out in the nucleus with an increase of 120 % compared to the cytoplasm. Furthermore, Zn-rich 250 nm sized features are spotted in the nucleus, outside the nucleoli, with a concentration up to 1.2 mM compared to the nuclear average of 0.52 mM. They are likely associated to zinc finger proteins.[40] An increase in Zn concentration by 41 % compared to the cytoplasm is observed as well in the Golgi compartment. The mass density changes are small, but noticeable. Compared to a density of exactly 1 g/cm^3 in the cytoplasm, the highest density is found in the nucleus (5 % increase), in particular in the nucleoli (9 % increase). Many vacuoles can be observed inside the cytoplasm. They stand out with a slightly higher density (2 % increase), whereas they are depleted in most elements compared to the other cell compartments. The mass density reconstructions show some sample preparation artefacts at the boundary of the vacuoles due to too slow freezing of the cells.[18] These artefacts are due to manual plunge-freezing. They can be avoided with standard fast freezing using an automatic plunge-freezing robot, that will increase the plunge velocity and enhance the vitrification quality. Despite, artefacts are regu-

larly observed depending on the cell thickness and the amount of blotting, which is of utmost importance to get a thin layer of vitreous ice embedding the cell.

The proposed technique provides 3D intracellular total molar elemental concentrations. Reported data of this kind are scarce, as intracellular concentrations for metal *free ions* are most often reported. For comparison, total cellular zinc amounts to 10^{-4} M in average that contrasts to the fM intracellular free Zn ions value.[41] This total Zn concentration is in agreement with our measured value in a macrophage cell (0.28 mM). To our knowledge, no values were reported for macrophages but only for phagosomes[42] and thus cannot be compared to our results. The measured cytosolic values remain in the expected average cellular elemental concentration range.[43] Typical cytosolic concentrations of potassium (K^+) and chlorine (Cl^-) were reported in the range of 140-155 and 5-15 mM respectively,[44] that are similar to the values reported here (121 and 19 mM respectively). Our Ca cytosolic concentration is very likely overestimatedcompared to the expected range of 10^{-4} mM. This is attributed to imperfections in the deconvolution of the overlapping potassium K_β and calcium K_α fluorescence signal.

In summary, we have demonstrated the combined use of cryo X-ray holographic and X-ray fluorescence nanotomography to reconstruct the 3D distributions of mass density and molar concentration of major and minor elements in entire frozen-hydrated macrophage cells. The quantification on a per organelle basis shows remarkable heterogeneity in the intracellular landscape. The correlative structural information provided by a phase contrast method on the same instrument is particularly relevant to interpret the elemental content in its cellular environment. This modality will benefit of further improvements in spatial resolution and sensitivity. In this context, the ongoing upgrade of the ESRF and future upgrade of other synchrotron facilities to higher spectral brightness is of particular interest.[45,46] In combination with faster detector and nanopositioning technology, the 3D correlative quantitative approach will be routinely applied to many cells, while preserving optimum resolution in 3D. This will foster many scientific applications in biology, such as metal homeostasis and drug transport, as well as in heterogeneous chemistry and catalysis.

Acknowledgement The ESRF is acknowledged for providing beamtime and support for the experiments at the nano-imaging beamline ID16A in the frame of proposal LS-2551.

Supporting Information Available

The supporting materials provide: (i) Animation video 1 showing projections for elements P-S-Cl-K-Ca-Mn-Fe-Zn; (ii) Animation video 2 showing slices of the molar concentration for elements P-S-Cl-K-Ca-Mn-Fe-Zn; (iii) Animation video 3 showing slices of the mass density; (iv) Animation video 4 showing volume renderings of the mass density distribution (gray), molar concentration of K (yellow), P (Samoan) and Zn (orange); (v) Animation video 5 comparing the reconstructed slices of the density, the Zn and P concentration, and the segmented compartments of the cell; (vi) Document on experimental setup, sample preparation, reconstruction of X-ray holographic nanotomography, reconstruction of X-ray fluorescence nanotomography, supplementary correlative cryo X-ray tomography results, and extended numerical values of the organelle quantification.

References

(1) Barber-Zucker, S.; Shaanan, B.; Zarivach, R. Transition metal binding selectivity in proteins and its correlation with the phylogenomic classification of the cation diffusion facilitator protein family. *Scientific reports* **2017**, *7*, 16381.

(2) Finney, L. A.; O'halloran, T. V. Transition metal speciation in the cell: insights from the chemistry of metal ion receptors. *Science* **2003**, *300*, 931–936.

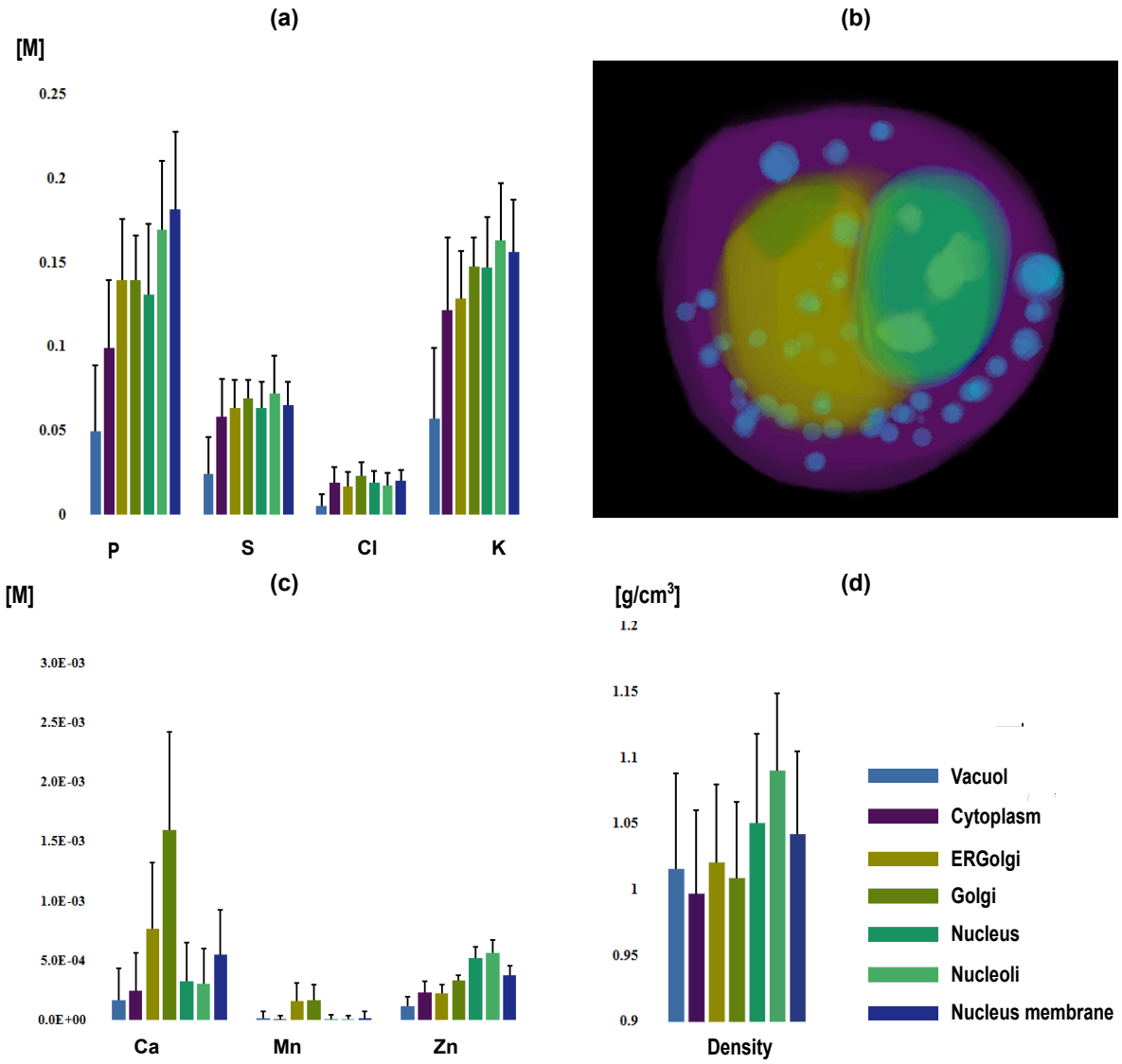

Figure 3: Quantification of the molar concentrations and mass density in different cell compartments. Average and standard deviation of (a) the molar concentrations of major elements P, S, Cl, K, (c) the molar concentrations of minor and trace elements Ca, Mn, Zn, and (d) the mass density. Note that the theoretical standard error of the mean is not shown as it is negligibly small. (b) 3D rendering of the segmented compartments consisting of the vacuoles, the cytoplasm (without vacuoles and ERGolgi), the system englobing the endoplasmic reticulum and Golgi apparatus, the Golgi apparatus, the nucleus (including the nucleoli and nuclear membrane), the nucleoli and the nuclear membrane.

(3) Lepanto, M. S.; Rosa, L.; Paesano, R.; Valenti, P.; Cutone, A. Lactoferrin in Aseptic and Septic Inflammation. *Molecules* **2019**, *24*, 1323.

(4) Milne, J. L.; Borgnia, M. J.; Bartesaghi, A.; Tran, E. E.; Earl, L. A.; Schauder, D. M.; Lengyel, J.; Pierson, J.; Patwardhan, A.; Subramaniam, S. Cryo-electron microscopy–a primer for the non-microscopist. *The FEBS journal* **2013**, *280*, 28–45.

(5) Da Cunha, M. M. L.; Trepout, S.; Messaoudi, C.; Wu, T.-D.; Ortega, R.; Guerquin-Kern, J.-L.; Marco, S. Overview of chemical imaging methods to address biological questions. *Micron* **2016**, *84*, 23–36.

(6) Aronova, M.; Leapman, R. Development of electron energy-loss spectroscopy in the biological sciences. *MRS bulletin* **2012**, *37*, 53–62.

(7) Messaoudi, C.; Aschman, N.; Cunha, M.; Oikawa, T.; Sorzano, C. O. S.; Marco, S. Three-dimensional chemical mapping by EFTEM-TomoJ including improvement of SNR by PCA and ART reconstruction of volume by noise suppression. *Microscopy and Microanalysis* **2013**, *19*, 1669–1677.

(8) Cavalier, A.; Spehner, D.; Humbel, B. M. *Handbook of cryo-preparation methods for electron microscopy*; CRC Press, 2008.

(9) Fletcher, J. S. Latest applications of 3D ToF-SIMS bio-imaging. *Biointerphases* **2015**, *10*, 018902.

(10) de Jonge, M. D.; Holzner, C.; Baines, S. B.; Twining, B. S.; Ignatyev, K.; Diaz, J.; Howard, D. L.; Legnini, D.; Miceli, A.; McNulty, I.; Jacobsen, C. J.; Vogt, S. Quantitative 3D elemental microtomography of Cyclotella meneghiniana at 400-nm resolution. *Proceedings of the National Academy of Sciences* **2010**, *107*, 15676–15680.

(11) Deng, J.; Lo, Y. H.; Gallagher-Jones, M.; Chen, S.; Pryor, A.; Jin, Q.; Hong, Y. P.; Nashed, Y. S.; Vogt, S.; Miao, J.; Jacobsen, C. Correlative 3D x-ray fluorescence and ptychographic tomography of frozen-hydrated green algae. *Science advances* **2018**, *4*, eaau4548.

(12) Gramaccioni, C.; Yang, Y.; Procopio, A.; Pacureanu, A.; Bohic, S.; Malucelli, E.; Iotti, S.; Farruggia, G.; Bukreeva, I.; Notargiacomo, A.; Fratini, M.; Valenti, P.; Rosa, L.; Berlutti, F.; Cloetens, P.; Lagomarsino, S. Nanoscale quantification of intracellular element concentration by X-ray fluorescence microscopy combined with X-ray phase contrast nanotomography. *Applied Physics Letters* **2018**, *112*, 053701.

(13) Yang, Y.; Fus, F.; Pacureanu, A.; da Silva, J.; De Nolf, W.; Biot, C.; Bohic, S.; Cloetens, P. Three-Dimensional Correlative Imaging of a Malaria-Infected Cell with a Hard X-ray Nanoprobe. *Analytical chemistry* **2019**, *91*, 6549.

(14) Stafford, S. L.; Bokil, N. J.; Achard, M. E.; Kapetanovic, R.; Schembri, M. A.; McEWAN, A. G.; Sweet, M. J. Metal ions in macrophage antimicrobial pathways: emerging roles for zinc and copper. 2013.

(15) Gao, H.; Dai, W.; Zhao, L.; Min, J.; Wang, F. The role of zinc and zinc homeostasis in macrophage function. *Journal of immunology research* **2018**, *2018*.

(16) Cairo, G.; Recalcati, S.; Mantovani, A.; Locati, M. Iron trafficking and metabolism in macrophages: contribution to the polarized phenotype. *Trends in immunology* **2011**, *32*, 241–247.

(17) Cutone, A.; Rosa, L.; Lepanto, M. S.; Scotti, M. J.; Berlutti, F.; di Patti, B.; Carmela, M.; Musci, G.; Valenti, P. Lactoferrin efficiently counteracts the inflammation-induced changes of the iron homeostasis system in macrophages. *Frontiers in Immunology* **2017**, *8*, 705.

(18) Skepper, J. Immunocytochemical strategies for electron microscopy: choice or compromise. *Journal of microscopy* **2000**, *199*, 1–36.

(19) da Silva, J. C.; Pacureanu, A.; Yang, Y.; Bohic, S.; Morawe, C.; Barrett, R.; Cloetens, P. Efficient concentration of high-energy x-rays for diffraction-limited imaging resolution. *Optica* **2017**, *4*, 492–495.

(20) Mokso, R.; Cloetens, P.; Maire, E.; Ludwig, W.; Buffière, J.-Y. Nanoscale zoom tomography with hard x rays using Kirkpatrick-Baez optics. *Applied physics letters* **2007**, *90*, 144104.

(21) Mirone, A.; Brun, E.; Gouillart, E.; Tafforeau, P.; Kieffer, J. The PyHST2 hybrid distributed code for high speed tomographic reconstruction with iterative reconstruction and a priori knowledge capabilities. *Nuclear Instruments and Methods in Physics Research Section B: Beam Interactions with Materials and Atoms* **2014**, *324*, 41–48.

(22) Guinier, A. *X-ray diffraction in crystals, imperfect crystals, and amorphous bodies*; Courier Corporation, North Chelmsford, MA, 1994.

(23) Seco, J.; Evans, P. M. Assessing the effect of electron density in photon dose calculations. *Medical physics* **2006**, *33*, 540–552.

(24) Sidky, E. Y.; Jørgensen, J. H.; Pan, X. Convex optimization problem prototyping for image reconstruction in computed tomography with the Chambolle-Pock algorithm. *Physics in Medicine and Biology* **2012**, *57*, 3065–3091.

(25) Viganò, N.; Solé, V. A. Physically corrected forward operators for induced emission tomography: a simulation study. *Measurement Science and Technology* **2017**, 1–26.

(26) Golosio, B.; Simionovici, A.; Somogyi, A.; Lemelle, L.; Chukalina, M.; Brunetti, A. Internal elemental microanalysis combining X-ray fluorescence, Compton and transmission tomography. *Journal of applied Physics* **2003**, *94*, 145–156.

(27) Bourassa, D.; Gleber, S.-C.; Vogt, S.; Yi, H.; Will, F.; Richter, H.; Shin, C. H.; Fahrni, C. J. 3D imaging of transition metals in the zebrafish embryo by X-ray fluorescence microtomography. *Metallomics* **2014**, *6*, 1648–1655.

(28) Di, Z. W.; Chen, S.; Hong, Y. P.; Jacobsen, C.; Leyffer, S.; Wild, S. M. Joint reconstruction of x-ray fluorescence and transmission tomography. *Optics express* **2017**, *25*, 13107–13124.

(29) Schindelin, J.; Arganda-Carreras, I.; Frise, E.; Kaynig, V.; Longair, M.; Pietzsch, T.; Preibisch, S.; Rueden, C.; Saalfeld, S.; Schmid, B. Fiji: an open-source platform for biological-image analysis. *Nature methods* **2012**, *9*, 676.

(30) Pettersen, E. F.; Goddard, T. D.; Huang, C. C.; Couch, G. S.; Greenblatt, D. M.; Meng, E. C.; Ferrin, T. E. UCSF Chimera—a visualization system for exploratory research and analysis. *Journal of computational chemistry* **2004**, *25*, 1605–1612.

(31) Bourne, G. H., Ed. *Division of Labor in Cells*, 2nd ed.; Academic Press, 1970; Chapter 6, pp 161 – 235.

(32) Legin, A. A.; Schintlmeister, A.; Jakupec, M. A.; Galanski, M.; Lichtscheidl, I.; Wagner, M.; Keppler, B. K. NanoSIMS combined with fluorescence microscopy as a tool for subcellular imaging of isotopically labeled platinum-based anticancer drugs. *Chem. Sci.* **2014**, *5*, 3135–3143.

(33) Schooley, A.; Vollmer, B.; Antonin, W. Building a nuclear envelope at the end of mitosis: coordinating membrane reorganization, nuclear pore complex assembly, and chromatin de-condensation. *Chromosoma* **2012**, *121*, 539–554.

(34) Lang, F.; Shumilina, E.; Ritter, M.; Gulbins, E.; Vereninov, A.; Huber, S. M. *Mechanisms and Significance of Cell Volume Regulation*; Karger Publishers, 2006; Vol. 152; pp 142–160.

(35) Yunos, N. M.; Bellomo, R.; Story, D.; Kellum, J. Bench-to-bedside review: chloride in critical illness. *Critical care* **2010**, *14*, 226.

(36) Feher, J. J. *Quantitative human physiology: an introduction*; Academic press, 2017.

(37) Chandra, S.; Kable, E.; Morrison, G. H.; Webb, W. W. Calcium sequestration in the Golgi apparatus of cultured mammalian cells revealed by laser scanning confocal microscopy and ion microscopy. *Journal of Cell Science* **1991**, *100*, 747–752.

(38) Pezzati, R.; Bossi, M.; Podini, P.; Meldolesi, J.; Grohovaz, F. High-resolution calcium mapping of the endoplasmic reticulum-Golgi-exocytic membrane system. Electron energy loss imaging analysis of quick frozen-freeze dried PC12 cells. *Molecular biology of the cell* **1997**, *8*, 1501–1512.

(39) Durr, G.; Strayle, J.; Plemper, R.; Elbs, S.; Klee, S. K.; Catty, P.; Wolf, D. H.; Rudolph, H. K. The medial-Golgi ion pump Pmr1 supplies the yeast secretory pathway with Ca2+ and Mn2+ required for glycosylation, sorting, and endoplasmic reticulum-associated protein degradation. *Molecular biology of the cell* **1998**, *9*, 1149–1162.

(40) Gamsjaeger, R.; Liew, C. K.; Loughlin, F. E.; Crossley, M.; Mackay, J. P. Sticky fingers: zinc-fingers as protein-recognition motifs. *Trends in biochemical sciences* **2007**, *32*, 63–70.

(41) Outten, C. E.; O'Halloran, T. V. Femtomolar sensitivity of metalloregulatory proteins controlling zinc homeostasis. *Science* **2001**, *292*, 2488–2492.

(42) Wagner, D.; Maser, J.; Lai, B.; Cai, Z.; Barry, C. E.; zu Bentrup, K. H.; Russell, D. G.; Bermudez, L. E. Elemental analysis of Mycobacterium avium-, Mycobacterium tuberculosis-, and Mycobacterium smegmatis-containing phagosomes indicates pathogen-induced microenvironments within the host cell's endosomal system. *The Journal of Immunology* **2005**, *174*, 1491–1500.

(43) Lodish, H.; Berk, A.; Kaiser, C. A.; Krieger, M.; Scott, M. P.; Bretscher, A.; Ploegh, H.; Matsudaira, P. *Molecular cell biology*; Macmillan, 2008.

(44) Alberts, B.; Wilson, J.; Hunt, T. Molecular Biology of the Cell (Garland Science, New York). *USA. 1601p* **2008**,

(45) Eriksson, M.; van der Veen, J. F.; Quitmann, C. Diffraction-limited storage rings – a window to the science of tomorrow. *Journal of Synchrotron Radiation* **2014**, *21*, 837–842.

(46) Raimondi, P. ESRF-EBS: The Extremely Brilliant Source Project. *Synchrotron Radiation News* **2016**, *29*, 8–15.

Graphical TOC Entry